Lab on a Chip

Accepted Manuscript

RSC Publishing

www.rsc.org/loc

Registered Charity Number 207890

Frequency tracking in acoustic trapping for improved performance stability and system surveillance

Björn Hammarström[1*], *Mikael Evander*[1], *Jacob Wahlström*[1], *and Johan Nilsson*[1]

[1]*Department of Measurement Technology and Industrial Electrical Engineering, Lund University, Sweden*

[*]*Bjorn.Hammarstrom@elmat.lth.se*

This work proposes and demonstrates an acoustic trapping system where the trapping frequency is automatically determined and can be used to analyse changes in the acoustic trap. Critical for the functionality of this system is the use of a kerfed transducer that removes spurious resonances. This makes it possible to determine the optimal trapping frequency by analysing electrical impedance. It is demonstrated that the novel combination of a kerfed transducer and acoustic trapping in glass capillaries creates a high Q-value resonator. This narrows the frequency bandwidth but allows excellent performance, as confirmed by a ten-fold increase in flow retention speed when compared to previously reported values. Importantly, the use of automatic frequency tracking allows the use of such a narrow bandwidth resonator without compromising system stability. As changes in temperature, buffer-properties, and the amount of captured particles will affect the properties of the acoustic resonator corresponding changes in resonance frequency will occur. It is shown that such frequency changes can be accurately tracked using the setup. Therefore, monitoring the frequency over time adds a new feature to acoustic trapping, where experimental progress can be monitored and the amount of trapped material can be quantified.

Introduction

Acoustic trapping allows non-contact retention of micro- and nanoparticles [1], a commonly needed and highly useful feature in lab on a chip systems [2]. The importance of accurate cell-capture and positioning in analysis is highlighted by the success of techniques such as patch clamp [3] and optical tweezers [4]. Allowing capture, retention and release of cells in microfluidic systems offers new experimental modalities and facilitates automation and integration of laboratory procedures. These respective advantages are highlighted in two articles, one featuring ultrasonically controlled positioning and aggregation during live cell imaging [5], and the other the use of acoustic differential extraction for automation of the manual procedure needed for DNA extraction in a forensic application [6]. In comparison to other techniques for micro scale particle capture, e.g. dielectrophoretic- or optical trapping, acoustic trapping stands out due to the fact that it allows application of large forces on population sizes ranging from single to several thousand cells [7], while maintaining viability [8-10] and functionality [11].

Acoustic trapping devices are commonly realized using acoustically resonating microstructures. Here, acoustic energy is stored in the resonator, allowing high field gradients and trapping forces to be utilized [12]. Alternative methods have been presented, such as acoustic trapping of micro particles in a high frequency ultrasonic beam [13, 14], or the use of surface acoustic waves (SAW) to dynamically position cells in a plane [15]. However, as recently demonstrated, dynamic positioning can be achieved in resonant devices by electrically controlling the position of actuation using patterned transducer electrodes [16]. Using low attenuating materials with high speed of sound (such as glass or silicon), and well-matched transducers, resonator devices can be made to have a high Q-value. Such designs build on the strengths of the

resonator-based approach, as a high Q-value implies that high acoustic energy is efficiently accumulated in the system. As the particle forces scale with the magnitude of the pressure and velocity gradients [17, 18], a system with high Q-value offers good performance in terms of sample throughput and capture rate without introducing excessive heating. Such devices are highly suitable for sample preparation applications such as enrichment or buffer exchanges where demands on throughput and capture performance are high. As recently demonstrated, acoustic trapping in rectangular cross-section class capillaries [19] provides straightforward means for realizing both enrichment of bacteria and nanoparticles [1] and highly efficient buffer exchange due to non-contact trapping and acoustic streaming properties [20].

A fundamental challenge in resonator-based devices is that any measure taken to optimize performance and create a high Q-value resonator will simultaneously narrow the frequency range in which the device can be operated (decreased bandwidth). For any system actuated at a fixed frequency this creates a trade-off between system stability and performance. Frequency-determining conditions, such as temperature and buffer properties, may change during operation, and as a highly optimized trap is very sensitive to such changes it runs a high risk failing and loose the trapped material. In buffer exchange experiments, where the media surrounding the captured bioparticles is replaced, a narrow frequency range limits the buffers that can be used, as their respective speed of sound has to match sufficiently such that a large shift in the system resonance frequency is not introduced. This trade-off creates severe limitations both in performance and in suitable application areas for acoustic trapping. Furthermore, if acoustic trapping is to have a major breakthrough as a lab tool or as an integrated part in laboratory equipment, manual frequency selection is undesirable, as it requires a skilled operator.

To address these challenges an automatic frequency tracking method based on impedance analysis of the ultrasonic transducer is proposed. In previous articles regarding acoustic particle manipulation impedance-based selection of the frequency has been suggested [21-23]. The primary challenge with this approach is unintentional selection of spurious resonance modes, these can arise either from unwanted resonances in the fluidic channel or in the transducer itself. Actuating a spurious resonance will produce little or no acoustic trapping and may sonicate parts of the device where no acoustic energy is desired. To solve this, we present a transducer fabrication method and a channel geometry that will reliably eliminate spurious modes in a several MHz-wide frequency range, and as experimentally verified, allows the use of impedance analysis to reliably select the correct trapping frequency.

By using a feedback system to continuously adjust the trapping frequency, performance stability can be achieved in spite of a narrow frequency band, effectively eliminating the trade-off between performance and stability. This is not only a crucial step in creating a robust and easy to use device, but monitoring changes in impedance and frequency can also be used to analyse changes in the acoustic trap. By studying frequency shifts in the acoustic trap over time, information about the in-situ temperature, buffer composition and trapped particles can be obtained. This adds a novel feature to the classic acoustic trap; not only enabling the quantification of the trapped material but also allowing buffer exchanges to be performed without being limited by the speed of sound in the different media. As the selected frequency is recorded continuously, experimental protocols will also receive specific frequency signatures that can be used for quality assurance without visually inspecting the acoustic trap.

Device fabrication

Acoustic trapping setup

Figure 1a shows the device used for non-contact acoustic trapping. As previously shown, localized actuation of a cross-sectional resonance in the capillary enables acoustic trapping [19]. A borosilicate capillary with 0.2×2 mm^2 cross-section

(VitroTubes, VitroCom, Mountain Lakes, NJ, USA) was used and actuated at the thickness mode close to 4 MHz. The localized actuation was achieved by using a miniaturized transducer fabricated as described below. Fluidic connections to the capillary were made by using elastic Tygon-tubing (R-3603 AAC00001,, Saint-Gobain S.A., Courbevoie, France) and UV-curable glue (Norland optical adhesive 68, Norland Products Inc., Cranbury, NJ, USA). A syringe pump (cetoni GmbH, Korbußen, Germany) was used to control the flow in the channel and samples were loaded in aspirate/dispense mode.

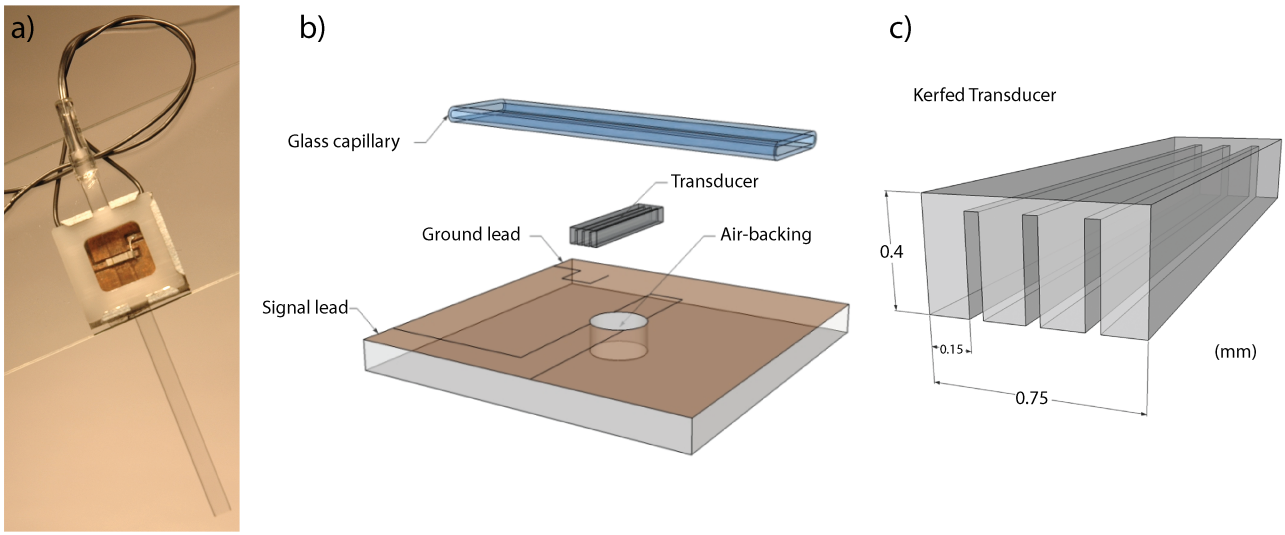

Figure 1: a) shows a photo of the assembled device used for acoustic trapping and b) shows an exploded view of the active region. Here, a kerfed 4 MHz transducer (mounted on a printed circuit board with a 1.5 mm air-backing hole) is brought into close contact with the capillary. c) shows a close-up of the kerfed transducer geometry with the 50 µm wide kerfs and 150 µm wide ridges.

Mode control in the piezoelectric element

To enable automatic frequency tracking, important modifications to the previously used miniaturized piezoelectric element [24-26] were made. Here, kerfing of the transducer element was employed to minimize the effects of spurious resonances (lateral modes).

The kerfed piezo element was cut from a 0.4 mm thick PZT-26 plate (Ferroperm Piezoceramics A/S, Kvistgaard, Denmark) with a silicon-dicing saw (Micro Automation Model 602M, General Signals, Inc, Evansville, IN, USA). The PZT-sheet was first diced using a 50 µm blade to form a smaller 3.2 mm wide plate. Subsequently it was rotated 90° and repeatedly cut leaving 10 µm of material to form 50 µm wide kerfs and 150 µm wide ridges. The desired number of ridges (4-6) was separated from the main block using a scalpel, leaving an element as depicted in figure 1c.

As the piezoelectric element was cut into thin ridges, the frequency of the thickness-mode resonance was reduced. This is a known phenomenon that occurs when a dimension is reduced to less than the wavelength in the piezoelectric material [27]. To compensate for the frequency shift, a 5 MHz sheet (0.4 mm thick) was used rather than a 4 MHz sheet (0.5 mm). For comparison, a piezoelectric element without kerfs was fabricated directly from a 0.5 mm sheet to form a solid $0.5 \times 0.8 \times 3.2$ mm^3 element.

The piezo elements were evaluated in an impedance analyzer (4194A Impedance/Gain-Phase Analyzer, Hewlett-Packard, Palo Alto, CA, USA) using a spring-loaded pin holder.

Mounting and assembly

The piezoelectric element was soldered, with the kerfs down, onto a 9 × 9 mm^2 printed circuit board (PCB) using low temperature solder-paste, figure 1b. The PCB provided electrical leads for the signal to the lower side of the transducer as well as a circular air-backing with a diameter of 1.5 mm. The transducer element was designed to be slightly wider than the capillary, such that electrical ground could be connected to the transducer element by soldering a thin silver wire from the top of the transducer down to the PCB ground terminal. Furthermore, the PCB dimensions were selected to comply with the 9 mm well pitch standard used in 96-well plates to allow easy side-by-side stacking for parallelization in future applications.

The capillary and the mounted transducer were assembled using an aluminum/polyoxymethylene holder with milled recessions for both the transducer-chip and the capillary. The holder was fabricated using a precision milling machine (ICP 4030, isel Germany AG, Eichenzell, Germany), ensuring correct alignment and a tight spacing between the piezoelectric element and the capillary. A thin film of glycerol was used to provide acoustic coupling between the capillary and the transducer.

Online impedance measurements

The device was actuated by a waveform generator (32220A, Agilent Technologies Inc, Santa Clara, CA, USA), see figure 2. The waveform generator was controlled through a LabVIEW program (National Instruments Corporation, Austin, TX, USA) over an USB-connection. The output from the waveform generator was connected to a peak detector circuit to monitor the voltage over the piezo. A description and circuit diagram of the peak detector can be found in the supplemental information. The output from the peak detector was connected to a data acquisition device (DAQ) (NI USB-6009, National Instruments Corporation, Austin, TX, USA) that was controlled through the same LabVIEW software, as was the waveform generator.

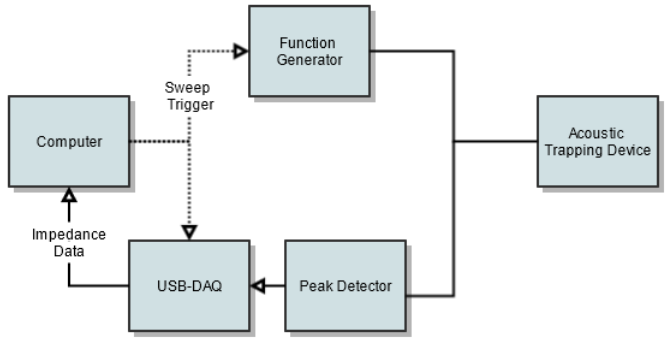

Figure 2: Block diagram describing the setup for continuous impedance acquisition.

To identify and track the optimal actuation frequency, the voltage over the piezo was measured during recurring frequency sweeps. The waveform generator was configured to perform a frequency sweep (± 5% around center frequency) after receiving an external trigger signal from the DAQ. The signal also triggered the data acquisition to collect amplitude data during the frequency sweep. The data from the DAQ was then processed in the software to identify the point of maximum

power input. The waveform generator settings were then updated to perform its continuous actuation at this frequency and wait for the next sweep.

The waiting time between frequency sweeps can be controlled through the software, as can the frequency range and the speed of the sweep. A 10 ms sweep was chosen, as it was short enough to not affect the trapping performance during continuous flow experiments. During the 10 ms frequency sweep, 200 data points were acquired using a sampling rate of 20 kS/s.

Experimental

Optimal trapping frequency

To investigate how the electrical resonance of the system correlated with the acoustical resonance in the capillary, the maximum retention flow was evaluated for a number of actuation frequencies. The acoustic trap was pre-loaded with a cluster of 3 μm polystyrene beads (80304 FLUKA, Sigma-Aldrich, St. Louis, MO, USA), and the fluid flow in the channel was increased in steps of 10 μL/min. The highest flow where beads could be retained was taken as a benchmark for trapping performance on that frequency.

An impedance spectrum for the device with a liquid filled channel was acquired using an impedance analyzer (4194A Impedance/Gain-Phase Analyzer, Hewlett-Packard, Palo Alto, CA, USA). The measured impedance spectrum together with knowledge of the output impedance of the function generator (50 Ω) as well as the set amplitude (10 V) allowed a power spectrum to be calculated.

Temperature changes

Thermal effects on the resonance frequency were evaluated by placing the entire setup in an incubator (KB 5260, Termaks, Bergen, Norway). The incubator was equipped with heating and cooling capabilities, allowing control of the ambient temperature. Temperatures from 15 to 45°C were evaluated. For each measurement, the system was allowed to stabilize for 2 min before the resonance frequency was measured once per second during 3 minutes.

Particle detection

A stock solution of 12-μm monodisperse polystyrene particles (88511 FLUKA, Sigma-Aldrich, St. Louis, MO, USA) was diluted 1:200 in deionized water and aspirated into the trapping capillary using a flowrate of 20 μL/min. Recording of the trapping frequency was started simultaneously with time-lapse image acquisition from a microscope and updated every second. This allowed the trapping frequency to be linked to an image frame where particles could be counted while retaining isoform buffer conditions. Prior to aspirating the polystyrene particles the trapping system was run for a few minutes to check that the selected frequency was constant, ensuring that a stable equilibrium temperature in the system was reached.

Buffer exchange with frequency tracking

The tubing and capillary was primed using 100 mM potassium chloride buffer (KCl) through a switch-valve using a syringe pump. 12-μm polystyrene particles (88511 FLUKA, Sigma-Aldrich, St. Louis, MO, USA) were then aspirated and

trapped to function as seed particles. When switching the valve, a sample of human plasma (containing low number of human red blood cells and platelets) was infused through the capillary at a flow rate of 10 µl/min. Cells were trapped and enriched in the seeding particle cluster. After 18 minutes, the valve was switched again to enable a 10-minute wash of the trapped cluster using 100 mM KCl at a flow rate of 10 µl/min. During the experiment, the frequency was tracked and logged every other second together with a time-lapse recording of the trapped cell cluster. Due to the volume in the tubing and valve used, there was a delay of about 100s before the plasma reached the trap and started affecting the system resonance.

Results and discussion

Device verification

Figure 3 shows the effect of transducer kerfing on the electrical impedance. The kerfed element (figure 3a) resembles a near-ideal 1D crystal oscillator with a large impedance dip at 4 MHz and a phase-shift close to 90° (with an anti-resonance close to 5 MHz). However, some minor reoccurring resonances can be observed that can probably be attributed to overtones to the 3.2 mm element length. In comparison, the solid transducer element (figure 3b) shows significant interference from the 2 MHz lateral-mode created by the 0.8 mm width. In this case, the spurious 2 MHz-mode dominates the spectrum both reducing the efficiency of the 4 MHz mode and causes interference with impedance based resonance tracking. For this setup, removal of the spurious modes through transducer kerfing is a necessary prerequisite for finding the correct resonance frequency through impedance analysis, and offers the potential to create a high Q-value resonator. This also demonstrates that removal of closely spaced modes is the most important, as the kHz-range modes from the 3.2 mm length has much less impact than the MHz-range modes from the 0.8 mm width. For this reason, mode control through kerfing is critical when two or more transducer dimensions are close. Therefore, one might anticipate that mode control will be more important for devices utilizing miniaturized transducers for localized actuation, than for macro scale devices utilizing large transducers where mode interference would be less of an issue.

Figure 3c shows the impedance spectrum of the mounted transducer. As seen from this spectrum most of the impedance characteristics from the free elements are preserved after mounting. The main effect of mounting the transducer on the PCB is the attenuation of resonance modes, as can be expected since acoustic losses into the PCB substrate are introduced. For frequency tracking, attenuation of the low frequency lateral modes from the 3.2 mm length is beneficial, as the packaged transducer is dominated by the 4-MHz thickness mode in a wide frequency band.

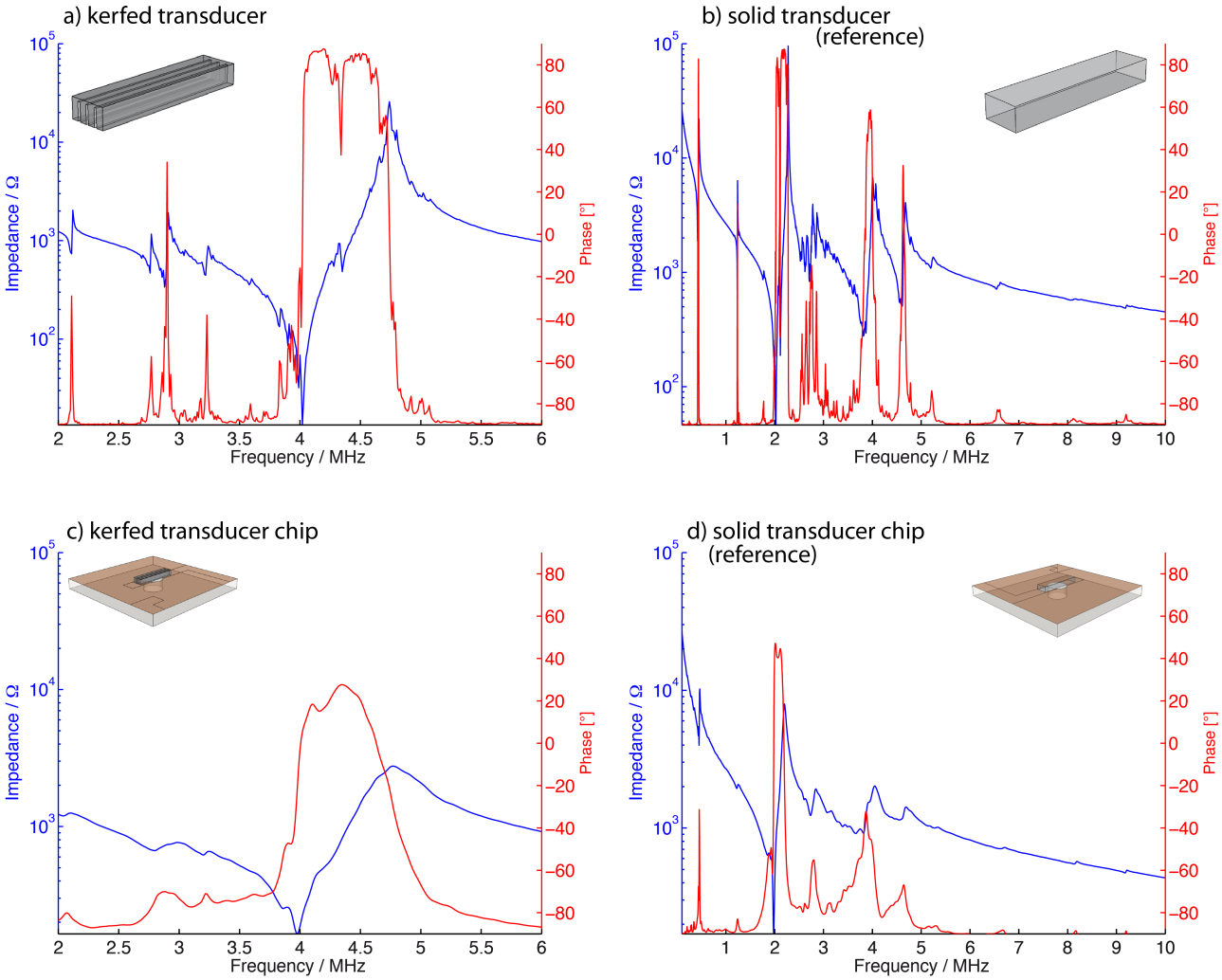

Figure 3: Impedance spectra for; a) a free kerfed transducer element before mounting, b) a free kerfless transducer block, c) a finished transducer chip using a kerfed transducer mounted on a PCB with 1.5 mm air-backing, and d) a mounted kerfless transducer block. The finished transducer chip is dominated by a clear resonance at 4 MHz, as shown by the large impedance dip and the zero phase transition. The kerfless transducer is included for reference only, as this shows the large lateral 2-MHz resonance that is removed by kerfing the transducer. When comparing mounted to free transducers, the attenuation of spurious modes from the 3.2 mm length of the transducer (reoccurring as closely spaced overtones to each fundamental) can also be observed. The impedance data shows that the presented fabrication method produces an actuator dominated by a single thickness resonance in a wide frequency band.

Optimal trapping frequency

The flow retention spectrum in figure 4 shows that the trapping performance was highly frequency dependent. If the frequency was selected correctly, the cluster could be retained at a flow as high as 500 µL/min, significantly higher than previously reported values [7]. However, selecting a frequency approximately 50 kHz off resonance resulted in a 10-fold decrease in performance.

When mounting the liquid filled capillary on the transducer, a noticeable change in the impedance spectrum was observed in comparison to an un-mounted transducer. The acquired impedance spectrum was used to calculate the power spectrum shown in figure 4, where the most noticeable effect was a shift of the power input maxima (corresponding to an impedance

minima). Comparing the power spectrum to the flow spectrum shows that the frequency with maximal power input coincides with the optimal trapping frequency. Six validation experiments of this using a capped maximum flow of 200 µL/min are available in supplementary information. The data shows that the capillary and the transducer interact acoustically to create a combined system resonance that can be determined by looking at the power-input. The acoustic coupling between the channel resonance and the transducer resonance can also be seen by looking at the relation between the retention flow and power. Seeing that the flow retention curve has higher Q-value (narrower bandwidth) than the power spectrum shows that the system not only has a higher power input but is also more efficiently actuated at the detected resonance.

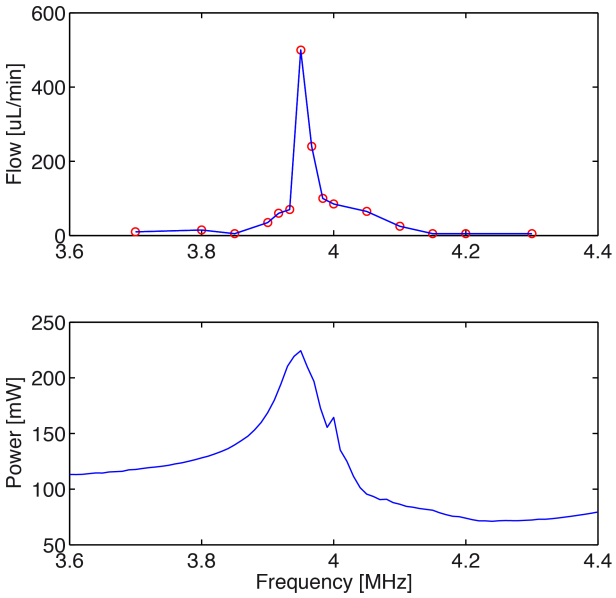

Figure 4: a) Shows the frequency dependence of the maximum flow at which a cluster of 3 µm beads can be retained in the trap. b) Shows the power input from the function generator as calculated from the impedance of the mounted system with capillary in place and beads in the channel. The coincidence between the optimal frequency for trapping and the maximum power input is indicated by the dashed line, and forms the basis for the frequency-tracking method.

Frequency tracking

Using the online impedance measurement setup described earlier, a power spectrum could be acquired every second. By selecting the frequency with maximal power input, the optimal trapping frequency could be updated continuously. In order to use more of the system information contained in the spectrum, a Gaussian curve was fitted to the data allowing an estimate of the Q-value of the system (as calculated from σ). Further, using the maxima of the fitted Gauss curve instead of the measured maxima ensured protection against accidental tracking of local maxima, one of which can be observed in the power spectrum in figure 4b close to 4-MHz.

A limitation to this model is that fitting a Gaussian curve implies that the crystal oscillator is modeled as a simple resonant circuit and thereby disregards the plate capacitance between the electrodes. This implies a flat baseline to the resonator where in reality there is a slope. This can be observed by the difference in baseline between left and right side of the resonance in figure 4b. However, if the sweep bandwidth is confined within 10% of the resonance a close agreement can be obtained. As the baseline is not included in the model, the calculated Q-value will depend on the sweep bandwidth and should therefore be interpreted as a relative measure of changes in the resonance quality and not as an absolute quantity.

More refined models, like the Mason model [28], are frequently used when modeling transducers for ultrasonic imaging and may provide room for determining the true electrical Q-value in future applications. However, as the calculation time between updates is limited, the simpler model was adopted as it still provides relevant data.

Temperature changes

The temperature dependence of the system resonance frequency is shown in figure 5. The temperature dependence is not entirely linear for the measured range (15 to 45 °C), where increasing the temperature from room temperature (RT) has a smaller influence than decreasing it. It is noted here that the speed of sound in water also has non-linear temperature dependence. However, this temperature dependence alone would not result in the exact frequency dependence observed in figure 5. This may suggest that, the resonance frequency is decided by the system as a whole (including glass walls and piezo) and not simply the liquid channel.

A measurable temperature dependence implies that the stability of the resonance frequency can be used to assess the stability of the in situ temperature. This has practical importance since monitoring a stable resonance frequency ensures that the in-trap temperature has reached equilibrium and is not, for instance, overheating due to a high actuation voltage. By creating a calibration curve such as in figure 5 one can also, for a specific set-up and sample, use the absolute frequency to gauge the in-trap temperature.

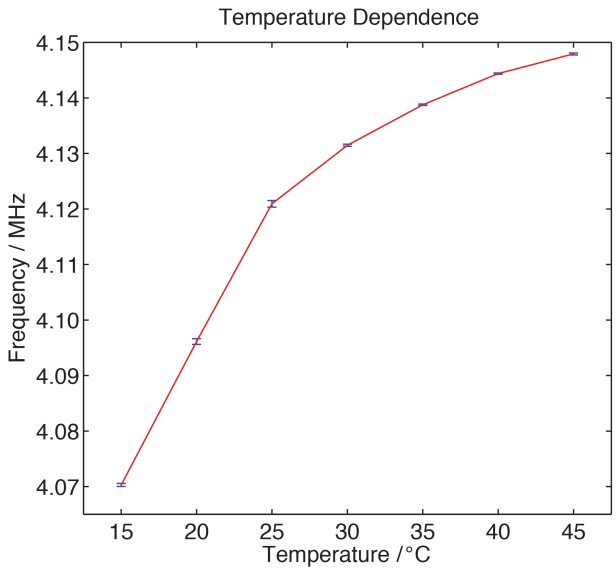

Figure 5: Temperature dependence for the system mounted with a water filled capillary in the 15-45 °C range.

Particle detection

By utilizing the feedback properties of the tracking system it was possible to detect captured particles by looking at how the frequency changed over time. As particles were captured the resonator properties were affected, and a frequency-shift was observed. During aspiration of 12-µm polystyrene particles, micrographs of the trapping region were acquired every second synchronously with updating the trapping frequency. By performing three replicates where a particle solution was aspirated and three replicates where a particle free solution was aspirated, the effects of particle capture was isolated from effects of temperature and media properties. Figure 6 shows the difference in average frequency between the particle

capture-runs and the reference-runs plotted from the time of first bead capture, as taken from the synchronous micrographs. To minimize noise, a moving average filter using 4 equally weighted samples was applied to the detection curve.

A constant decrease in trapping frequency occurred during particle capture. As a constant flow rate and sample concentration was maintained during the experiment, a linear frequency-shift is expected if directly correlated to the amount of trapped beads. The insets in figure 6 are micrographs correlated with the frequency shift after 25, 50 and 150 seconds of capture, showing a continuous increase in the number of trapped beads. As seen here, the beads form a close packed structure held together by the acoustic forces. A supplemental video of the trapping is available, showing that when a critical number of beads are trapped the cluster begins to rearrange from a monolayer to a double or triple layer. The formation of double or triple stacked layers makes an absolute quantification through microscopic images very challenging. However, an estimation of the frequency shift per bead can be gleaned by studying the image taken after 25 seconds. Here, a frequency shift of 0.5 kHz can be discerned and no double stacking of the 12-µm particles has yet occurred. This allows the beads to be manually counted resulting in approximately 500 beads, i.e. a frequency shift in the order of 1 Hz/bead.

Marston et al has previously discovered that a resonance frequency shift can be induced by microparticle migration in an acoustic field [22]. This work was performed in a large-scale closed container and provides a thorough theoretical description of the mechanism behind the frequency shift. Briefly, the resonance shift is determined by particle position, volume, compressibility and density. Our work combines these findings with a working device for acoustic trapping and utilizes the effect to monitor a locally increasing bead concentration.

From an application perspective, induced resonance shift in acoustic trapping resembles the widely used quartz crystal microbalance (QCM) technique. Here, material is chemically captured onto the surface of a piezoelectric resonator [29, 30] and causes a detectable frequency shift. In QCM the observed frequency shift is attributed to mass loading of the resonator and most simply described by the Sauerbrey equation that states a linear decrease in frequency with added mass. While QCM may be a more developed and sensitive system, the acoustic trapping method has the advantage to be integrated with a capture mechanism and offers the ability to address compressibility as well.

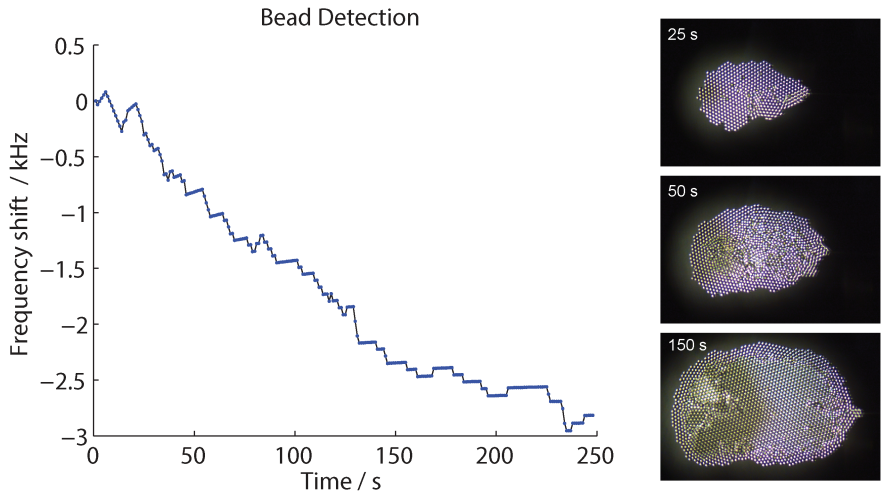

Figure 6: Shift in the tracked frequency as a function time during accumulation of 12-µm beads, the insets shows stills captured synchronously with updating the frequency.

Buffer exchange with frequency tracking

The experiment starts with a cluster of 12 µm seeding particles suspended in 100 mM KCl, as can be seen in the inset image labeled "60 s" in figure 7. As the human plasma reaches the capillary, a gradual increase in the optimal trapping frequency can be clearly seen in the tracking software, see figure 7. During the 1080 s of plasma infusion, a gradual decrease in the trapping frequency can be seen as the amount of cells in the trapped cluster increases. This can also be seen in the pictures from the timelapse-recording in figure 7. When the KCl-washing starts at 1100 s, a clear decrease in frequency can be seen as the plasma is washed away. When comparing the starting frequency with the frequency after the trapping and washing, a frequency shift, correlating to the amount of cells trapped, can be seen. This is the same behavior as observed in the particle detection experiments, only here there is an added frequency shift caused by the buffer exchange.

By using frequency tracking, it is possible to maintain optimal trapping conditions during these kinds of experiments where the resonance frequency of the system changes without the risk of losing trapped particles or compromising the trapping efficiency, compare to figure 4a.

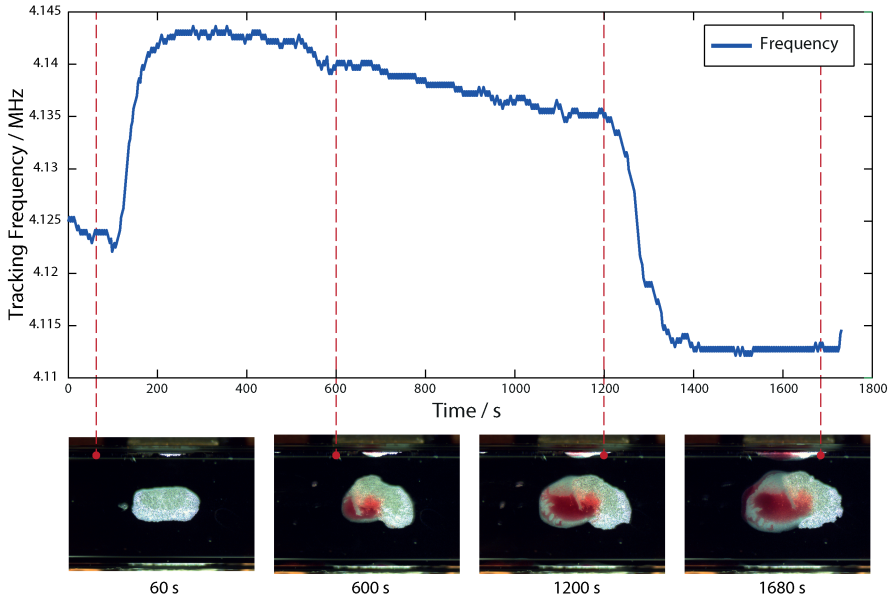

Figure 7: A plot showing how the optimal trapping frequency changes when switching between wash buffer and sample. Initially the capillary is filled with KCl and a cluster of 12-µm polystyrene seeding particles. At 200 s, human plasma is infused until 1100 s where the plasma is washed away using KCl. A clear change in frequency can be seen during the media switches as well as a gradual decrease in frequency during the sample infusion as the amount of trapped cells increases.

Conclusions

This work presents a straightforward and low cost fabrication method for ultrasonic transducers that enables resonance tracking in acoustic trapping. Utilizing a kerfed transducer minimizes spurious resonances, and enables the use of impedance analysis for optimal trapping frequency determination. Characterization of the trapping performance and impedance properties of the assembled device shows that optimal conditions for trapping coincide with the frequency that has most efficient power conversion.

Continuously updating the operation frequency allows the acoustic trap to adjust to changes in temperature and buffer conditions. This creates a robust device that can be used in a wider range of applications as constrictions on matching sample and buffers are removed. A frequency-tracked acoustic trap also allows the use of a less attenuated system (high Q-value), as a narrow frequency operation span does not compromise the system stability. In a well-characterized system a frequency tracked acoustic trap can be used as a sensor capable of accessing changes in buffer properties, temperature and amount of trapped material.

Acknowledgements

The research leading to these results has received funding form the European Union Seventh Framework Programme (FP7/2007-2011) under grant agreement n° 259848. The authors would like to greatly acknowledge The Swedish Research Council (Dnr. 621-2010-4389) for financial support.

References

1. Hammarstrom, B., T. Laurell, and J. Nilsson, *Seed particle enabled acoustic trapping of bacteria and nanoparticles in continuous flow systems.* Lab on a Chip, 2012.

2. Evander, M. and J. Nilsson, *Acoustofluidics 20: Applications in acoustic trapping.* Lab on a Chip, 2012. **12**(22): p. 4667-4676.

3. Neher, E. and B. Sakmann, *Single-Channel Currents Recorded from Membrane of Denervated Frog Muscle-Fibers.* Nature, 1976. **260**(5554): p. 799-802.

4. Ashkin, A. and J.M. Dziedzic, *Optical Trapping and Manipulation of Viruses and Bacteria.* Science, 1987. **235**(4795): p. 1517-1520.

5. Christakou, A.E., et al., *Live cell imaging in a micro-array of acoustic traps facilitates quantification of natural killer cell heterogeneity.* Integrative Biology, 2013. **5**(4): p. 712-719.

6. Norris, J.V., et al., *Acoustic Differential Extraction for Forensic Analysis of Sexual Assault Evidence.* Analytical Chemistry, 2009. **81**(15): p. 6089-6095.

7. Nilsson, J., et al., *Review of cell and particle trapping in microfluidic systems.* Analytica Chimica Acta, 2009. **649**(2): p. 141-157.

8. Evander, M., et al., *Noninvasive acoustic cell trapping in a microfluidic perfusion system for online bioassays.* Analytical Chemistry, 2007. **79**(7): p. 2984-2991.

9. Hultstrom, J., et al., *Proliferation and viability of adherent cells manipulated by standing-wave ultrasound in a microfluidic chip.* Ultrasound in Medicine and Biology, 2007. **33**(1): p. 145-151.

10. Bazou, D., L.A. Kuznetsova, and W.T. Coakley, *Physical enviroment of 2-D animal cell aggregates formed in a short pathlength ultrasound standing wave trap.* Ultrasound in Medicine and Biology, 2005. **31**(3): p. 423-430.

11. Bazou, D., et al., *Gene expression analysis of mouse embryonic stem cells following levitation in an ultrasound standing wave trap.* Ultrasound Med Biol. **37**(2): p. 321-30.

12. Lenshof, A., et al., *Acoustofluidics 5: Building microfluidic acoustic resonators.* Lab on a Chip, 2012. **12**(4): p. 684-695.

13. Lee, J., et al., *Single beam acoustic trapping.* Applied Physics Letters, 2009. **95**(7).

14. Zheng, F., et al., *Acoustic trapping with a high frequency linear phased array.* Applied Physics Letters, 2012. **101**(21).

15. Ding, X.Y., et al., *On-chip manipulation of single microparticles, cells, and organisms using surface acoustic waves.* Proceedings of the National Academy of Sciences of the United States of America, 2012. **109**(28): p. 11105-11109.

16. Glynne-Jones, P., et al., *Array-Controlled Ultrasonic Manipulation of Particles in Planar Acoustic Resonator.* Ieee Transactions on Ultrasonics Ferroelectrics and Frequency Control, 2012. **59**(6): p. 1258-1266.

17. Gorkov, L.P., *Forces Acting on a Small Particle in an Acoustic Field within an Ideal Fluid.* Doklady Akademii Nauk Sssr, 1961. **140**(1): p. 88-&.

18. Bruus, H., *Acoustofluidics 7: The acoustic radiation force on small particles.* Lab on a Chip, 2012. **12**(6): p. 1014-1021.

19. Hammarstrom, B., et al., *Non-contact acoustic cell trapping in disposable glass capillaries.* Lab on a chip, 2010. **10**(17): p. 2251-2257.

20. Hammarstrom, B., et al., *Efficient sample preparation in immuno-matrix-assisted laser desorption/ionization mass spectrometry using acoustic trapping.* Biomicrofluidics, 2013. **7**(2).

21. Dual, J., et al., *Acoustofluidics 6: Experimental characterization of ultrasonic particle manipulation devices.* Lab on a Chip, 2012. **12**(5): p. 852-862.

22. Kwiatkowski, C.S. and P.L. Marston, *Resonator frequency shift due to ultrasonically induced microparticle migration in an aqueous suspension: Observations and model for the maximum frequency shift.* Journal of the Acoustical Society of America, 1998. **103**(6): p. 3290-3300.

23. Hawkes, J.J. and W.T. Coakley, *A continuous flow ultrasonic cell-filtering method.* Enzyme and Microbial Technology, 1996. **19**(1): p. 57-62.

24. Lilliehorn, T., et al., *Dynamic arraying of microbeads for bioassays in microfluidic channels.* Sensors and Actuators B-Chemical, 2005. **106**(2): p. 851-858.

25. Lilliehorn, T., et al., *Trapping of microparticles in the near field of an ultrasonic transducer.* Ultrasonics, 2005. **43**(5): p. 293-303.

26. Johansson, L., et al., *An evaluation of the temperature increase from PZT micro-transducers for acoustic trapping.* 2005 IEEE Ultrasonics Symposium, Vols 1-4, 2005: p. 1614-1617.

27. Cobbold, R.S., *Foundations of biomedical ultrasound*. 2007: Oxford University Press New York:.

28. Ritter, T., et al., *Electromechanical properties of thin strip piezoelectric vibrators at high frequency.* Journal of Applied Physics, 2000. **88**(1): p. 394-397.

29. Wegener, J., A. Janshoff, and C. Steinem, *The quartz crystal microbalance as a novel means to study cell-substrate interactions in situ.* Cell Biochem Biophys, 2001. **34**(1): p. 121-51.

30. Hook, F., et al., *Structural changes in hemoglobin during adsorption to solid surfaces: effects of pH, ionic strength, and ligand binding.* Proc Natl Acad Sci U S A, 1998. **95**(21): p. 12271-6.